PERGAMON

International Journal of Heat and Mass Transfer 46 (2003) 989–997

International Journal of HEAT and MASS TRANSFER

www.elsevier.com/locate/ijhmt

Transient non-isothermal behavior during the growth and collapse of spherical fluid shells

Xundong Qin [a], Roger E. Khayat [a,*], Ky T. Nguyen [b]

[a] *Department of Mechanical and Materials Engineering, Faculty of Engineering Science, The University of Western Ontario, London, Ont., Canada, N6A 5B9*

[b] *Department of Mechanical Engineering, Ecole Polytechnique de Montreal, Montreal, Que., Canada, H3C 3A7*

Received 6 July 2001; received in revised form 3 September 2002

Abstract

This theoretical study explores the influence of inertia, surface tension, and viscous dissipation on the transient heat transfer during the growth and collapse of fluid shells. The shell is spherical, the fluid is Newtonian, and the flow is induced by a constant driving pressure. The coupled heat and flow equations are solved numerically using the Cobody (Lagrangian) transformation and a central difference discretization in space. The results are described in terms of four dimensionless numbers, namely, the Reynolds number, the capillary number, the Peclet number and the Brinkman number. In particular, it is found that viscous dissipation and surface tension have a significant effect on the temperature evolution within the fluid, namely on the temperature buildup within the fluid shell.

1. Introduction

Research on the growth and collapse of shells and bubbles has a long history. The problem is of considerable fundamental interest in transport phenomena as an example of time-dependent free-boundary problem involving the interaction among heat, mass and momentum transfer. This flow configuration also enjoys several practical applications in industrial processes such as the manufacture of foam and microcellular materials [1], and can be related to blow molding and thermoforming [2].

Microcellular polymers are foam material with cell sizes of less than or equal to 10 μm. They are used in a wide variety of applications such as separation media, adsorbents, controlled release devices and light-weight materials with impact strength [3]. In forming a microcellular material, a gas such as carbon dioxide (CO_2) is first dissolved into a molten polymer under supercritical conditions, i.e., above the CO_2's critical temperature and pressure, to form a homogeneous polymer solution. Phase separation is then induced by either reducing sharply the pressure or the temperature resulting in the nucleation of a myriad of gas bubbles. The size of the final bubbles depends on several factors such as the number of nucleation sites, the initial gas concentration, the growth dynamics of the bubbles, the polymer properties such as diffusion coefficient, viscosity, elasticity, etc. The theoretical problem of predicting the cell size in foam materials is extremely complex. Some of the specific issues are described below.

One of the fundamental problems is the pressure history in the bubble. Initially, the fluid has to be at high pressure so that nucleation is prevented. Phase separation will start when the pressure falls below a certain threshold. Therefore, the initial pressure in the gas bubble can be taken as the threshold pressure. The difference between the initial fluid pressure and the threshold pressure provides the driving force for the bubble growth. This is the typical approach of earlier researchers. However, this is only the initial driving force. Once the bubble starts to grow, this driving pressure will certainly change, which has to be determined from the diffusion of gas into the bubble. The

* Corresponding author. Tel.: +1-519-661-2111/514-661-2111x88253; fax: +1-519-661-3020/514-661-3020.

E-mail address: rkhayat@eng.uwo.ca (R.E. Khayat).

0017-9310/03/$ - see front matter
PII: S0017-9310(02)00376-9

Nomenclature

Br	Brinkman number
C_P	heat capacity at constant pressure, J/(Kg K)
Ca	capillary number
k	thermal conductivity, W/(cm K)
N	number of nodes
P	dimensionless pressure
Pe	Peclet number
r	dimensionless radial position
R	dimensionless radius of inner shell surface
R_0	initial radius of the bubble, cm
Re	Reynolds number
R_r	initial outer to inner radius ratio
S	dimensionless radius of outer shell surface
t	dimensionless time
t'	dimensionless time from Lagrangian transformation
T	dimensionless temperature
T_{max}	dimensionless maximum temperature
T_0	reference temperature, K
u	dimensionless radial velocity
$\mathbf{u}$	velocity vector, cm/s
x	dimensionless Lagrangian coordinate position
x_i	dimensionless Lagrangian coordinate position at ith node
Δ	dimensionless mesh size
ΔP	dimensionless driving pressure
γ	surface tension coefficient, dyne/cm
μ	viscosity, g/(cm s)
ρ	density, g/m^3

Subscripts

r	partial differentiation with respect to radial position
t	partial differentiation with respect to time

pressure history in the bubble will then depend on the mass of material accumulated inside, its temperature and the size of the bubble.

Another problem is the effect of viscoelasticity on the growth of the bubble. Even though many researchers agree on some general behavior, the results vary widely with the choice of constitutive equations. One of the difficulties with viscoelasticity is a larger set of equations to be solved and the breakdown of the solution at a finite level of elasticity [4]. Besides viscoelasticity, the viscosity of the material is also of particular importance, especially the elongational viscosity since the deformation in the bubble is essentially biaxial. The inflation dynamics of a spherical shell is similar to that of the growth or collapse of a spherical gas bubble in an infinite Newtonain or viscoelastic medium; a spherical bubble is just a spherical shell of infinite thickness. Both configurations give rise to biaxial elongational flow. Fogler and Goddard [5] analyzed the decay of a bubble, initially at rest and later subject to a constant driving pressure for a Maxwell fluid. The elasticity of the fluid surrounding the spherical bubble was found to retard the collapse of the bubble and give rise to a time oscillatory behavior that is absent for a Newtonian fluid. It was also found that the oscillatory motion is particularly enhanced whenever the relaxation time is large compared to the Rayleigh collapse time, i.e., at large Deborah number. Tanasawa and Yang [6], and Ting [7] used a three-parameter Oldroyd model [8] and predicted a similar behavior. Pearson and Middleman [9,10] and later Johnson and Middleman [11] measured the decay of a bubble, subjected to an initial sudden pressure drop, collapsing in a large polymeric melt. The evolution of the bubble radius was monitored and was found to decay monotonically as in the case of a purely Newtonian fluid. Inertial effects were neglected and no oscillatory behavior was predicted. However, the calculations of Khayat and Garcia-Rejon [12] for a viscoelastic fluid confirm that, had inertia effects been included in Refs. [9–11], the resulting decay of the bubble radius would have been oscillatory.

Oscillations in statically stressed (that is, under constant driving pressure) viscoelastic fluids, which are absent for Newtonian fluids, are the result of normal stresses (which lead to the Weissenberg rod-climbing phenomenon [8]). Recent theoretical and experimental works on polymer melts and solutions give ample evidence of the existence of oscillatory behavior [12]. The discrepancy between theory and the experiments of Middleman and co-workers [9–11], particularly the fact that theoretically predicted oscillations are not observed in reality, is fundamentally important to understand. Recently, Khayat [13] addressed the origin of the discrepancy between theory and experiment for statically stressed systems. In particular, the work focused on the inflation of a spherical shell of a viscoelastic liquid subject to a time-dependent driving pressure.

Other aspects such as compressibility, gas diffusion and non-isothermal influences are also important, but have been largely ignored in the literature [14,15]. Earlier, Barlow and Langlois [16] examined the gas diffusion from a Newtonian fluid into an expanding bubble. Street et al. [17] examined the growth of a gas bubble in viscous power-law liquids considering the effect of heat, mass, and momentum transfer. In relation to foam molding, Han and Yoo [18] modeled the expansion foam by

considering the growth of a single bubble in an infinite liquid medium, and conducted experiments as well. Amon and Denson [19,20] introduced a cell model to account for the depletion of gas, with finite amount of liquid being stretched during the bubble expansion in foam processing. More recently, Arefmanesh and Advani [21] carried out a numerical study based on a polynomial representation of the gas concentration around the bubble under isothermal situations.

Non-isothermal effects have received very little attention despite their impact on bubble and shell dynamics. Arefmanesh and Advani [22] examined the non-isothermal bubble growth in polymeric foams. There was, however, essentially no discussion of the actual heat transfer involved. Moreover, the important dissipative mechanism in the energy was neglected. In this study, a systematic theoretical work is attempted to assess the impact of inertia, convection, dissipation and surface tension on the heat transfer during the growth and collapse of spherical shells of Newtonian fluids. The problem is formulated in Section 2, and the solution procedure is also presented in that section. The influence of the various parameters in the problem is examined in detail in Section 3. Concluding remarks are given in Section 4.

2. Problem formulation and solution procedure

The general equations for a Newtonian fluid spherical shell with the boundary and initial conditions, and the solution procedure are presented in this section. Given the symmetry of the flow, the problem reduces to a transient one-dimensional flow.

2.1. General equations

The fluid is assumed to be incompressible of density ρ, viscosity μ, surface tension coefficient γ, heat capacity C_p, and thermal conductivity k. These properties are assumed to be constant. The flow is induced by the action of a constant driving pressure acting on the inner shell surface. The temperatures are assumed fixed at the inner and outer surfaces. The governing equations are cast in dimensionless form. Let ΔP be the magnitude of the constant driving pressure so that the reference velocity is $V = (\Delta P/\rho)^{1/2}$. The reference length and time are, respectively, the initial radius R_0 of the inner shell surface and R_0/V, while the temperature, T_0, at the outer surface is taken as the reference temperature. The pressure is non-dimensionalized with respect to ρV^2.

The conservation of mass and momentum equations, as well as energy equation may be, respectively, written generally in dimensionless forms as

$$\nabla \cdot \mathbf{u} = 0, \tag{1}$$

$$Re\left(\frac{\partial \mathbf{u}}{\partial t} + \mathbf{u}\cdot\nabla\mathbf{u}\right) = -Re\nabla p + \nabla^2\mathbf{u}, \tag{2}$$

$$Pe\left(\frac{\partial T}{\partial t} + \mathbf{u}\cdot\nabla T\right) = \nabla^2 T + Br\nabla\mathbf{u} : \nabla\mathbf{u}, \tag{3}$$

where ∇ is the gradient operator, t is the time, T is the temperature, p is the pressure, and $\mathbf{u}$ is the velocity vector. There are five dimensionless groups in the problems, namely the Reynolds number, Re, Peclet number, Pe, Brinkman number, Br, capillary numbers, Ca, as well as the initial outer-to-inner surface radius ratio, R_r. These are explicitly and respectively given by

$$Re = \frac{\rho V R_0}{\mu}, \quad Pe = \frac{R_0 V \rho C_p}{k}, \quad Br = \frac{\mu V^2}{kT_0}, \quad Ca = \frac{\mu V}{\gamma}, \quad R_r = \frac{S_0 - R_0}{R_0}, \tag{4}$$

where S_0 is the initial radius of the outer shell surface.

2.2. Problem formulation

Consider the fluid at any time t occupying the region of a spherical shell of inner and outer radii $R(t)$ and $S(t)$, respectively. The flow is assumed to be spherically symmetric, thus reducing to a transient one-dimensional problem in the radial direction, r. More explicitly, the conservation of mass and momentum as well as energy Eqs. (1)–(3) reduce to

$$u_r + 2\frac{u}{r} = 0, \tag{5}$$

$$Re(u_t + uu_r) = -Rep_r + 2u_{rr} + \frac{2}{r}\left(u_r - \frac{u}{r}\right), \tag{6}$$

$$Pe(T_t + uT_r) = \frac{2}{r}T_r + T_{rr} + 2Br\left[u_r^2 + 2\left(\frac{u}{r}\right)^2\right], \tag{7}$$

where u is the radial velocity component. A subscript denotes partial differentiation.

The boundary conditions for the problem are imposed on the shell surfaces. The dynamic condition gives

$$-Rep(R,t) + 2u_r(R,t) - \frac{2}{\mathrm{CaR}(t)} = -Re \quad \forall t > 0, \tag{8a}$$

$$-Rep(S,t) + 2u_r(S,t) + \frac{2}{\mathrm{CaS}(t)} = 0 \quad \forall t > 0. \tag{8b}$$

In the present work, the air inside the shell is assumed to be motionless. The dynamic boundary conditions (8) are derived under equilibrium conditions. Their validity under dynamics conditions is usually simply assumed. For further discussion on the validity of this assumption, the reader is referred to [23,24]. The kinematic conditions simply reduce to

$$u(r = R, t) = \dot{R}, \; u(r = S, t) = \dot{S} \quad \forall t > 0. \tag{9}$$

The temperature is also prescribed at the inner and outer shell surfaces, such that

$$T(r=R,t)=2,\ T(r=S,t)=1 \quad \forall t>0. \tag{10}$$

Finally, regarding the initial conditions, the fluid is assumed to be initially at rest:

$$u(r,t\leqslant 0)=0 \quad \forall r\in[1,R_r]. \tag{11}$$

The temperature is assumed to obey the steady-state distribution that satisfies conditions (10). In other words,

$$T(r,t\leqslant 0)=\left(\frac{R_r+1}{R_r}\right)\frac{1}{r}+\frac{R_r-1}{R_r}. \tag{12}$$

The problem is now reduced to an initial-value system.

2.3. Reduced equations

The integration of Eq. (5) and use of conditions (9) lead to the following expressions:

$$u(r,t)=\frac{\dot{R}(t)R^2(t)}{r^2}=\frac{\dot{S}(t)S^2(t)}{r^2} \quad \forall r\in[R(t),S(t)]. \tag{13}$$

Integration of Eq. (6) over r between the inner and outer surfaces, and eliminating the pressure from conditions (8) and the radial velocity component from (13), lead to

$$Re\left[R(R\ddot{R}+2\dot{R}^2)\left(\frac{1}{R}-\frac{1}{S}\right)-\frac{1}{2}(R^2\dot{R})^2\left(\frac{1}{R^4}-\frac{1}{S^4}\right)\right]$$
$$=Re-\frac{2}{Ca}\left(\frac{1}{R}+\frac{1}{S}\right)+4\dot{R}\left(\frac{R^2}{S^3}-\frac{1}{R}\right), \tag{14}$$

where it is observed, from (13), that the evolution of the outer surface radius is related to $R(t)$ through

$$S(t)=[R(t)^3-1+(R_r+1)^3]^{1/3}. \tag{15}$$

The energy Eq. (7) is accordingly reduced to

$$Pe\left(T_t+\frac{\dot{R}R^2}{r^2}T_r\right)=\frac{2}{r}T_r+T_{rr}+12Br\left(\frac{\dot{R}R^2}{r^3}\right)^2. \tag{16}$$

2.4. Solution procedure

The energy Eq. (15) is recast in terms of Langrangian coordinates (x,t') according to the transformation

$$r=(x+R^3)^{1/3},\quad t=t', \tag{17}$$

which is originally due to Epstein and Plesset [25]. This transformation is useful as it allows the spatial integration to be carried out over a fixed interval $x\in\lfloor 0,(R_r+1)^3-1\rfloor$ as opposed to the time-dependent interval $r\in[R(t),S(t)]$. Furthermore, the transformation allows the elimination of the convective term, such that

$$PeT_t=12(x+R^3)^{1/3}T_x+9(x+R^3)^{4/3}T_{xx}+12Br\frac{R^4\dot{R}^2}{(x+R^3)^2}, \tag{18}$$

where the prime is dropped in the time. Eq. (18) is reduced to a set of ODEs by using a implicit central difference discretization along x. Thus,

$$Pe\frac{dT_i}{dt}=12(x_i+R^3)^{1/3}\frac{T_{i+1}-T_{i-1}}{2\Delta}+9(x_i+R^3)^{4/3}$$
$$\times\frac{T_{i+1}-2T_i+T_{i-1}}{(2\Delta)^2}+12Br\frac{R^4\dot{R}^2}{(x_i+R^3)^2}, \tag{19}$$

where T_i is the temperature at the ith node positioned at x_i. Here $\Delta=x_{i+1}-x_i$ is the mesh size. It turned out that a fixed increment, $\Delta=(R_r+1)^3-1/N$, was entirely sufficient to obtain numerical stability in the solution procedure, where N is the number of the nodes.

Upon substitution for S from Eq. (15), the system of Eqs. (14) and (19) constitute an initial-value problem with $N+2$ degrees of freedom, with initial conditions as follows. The initial radii of the inner and outer surfaces of the shell are fixed such that

$$R(t=0)=1. \tag{20}$$

Since the fluid is initially at rest, then

$$\dot{R}(t=0)=0. \tag{21}$$

The initial values for T_i follow from condition (12) and transformation (17), to give

$$T_i(t=0)=\left(\frac{R_r+1}{R_r}\right)(i\Delta+R^3)^{-1/3}$$
$$+\frac{R_r-1}{R_r},\quad i\in[1,N]. \tag{22}$$

A sixth-order Runge–Kutta scheme (IMSL-DIVPRK) is applied to integrate system (14) and (19). The accuracy of the solution was checked using Gear's predictor–corrector method (IMSL-DIVPAG). The results from both methods are essentially identical when the same time increment is used. In both methods, a tolerance of less than 10^{-6} is used. That is, the norm of the local error is controlled such that the global error is less than the tolerance imposed. Additional accuracy assessment is reported below.

3. Discussion and results

In this section, the evolution of the flow field and the simultaneous heat convection are determined for a spherical shell subject to a constant driving pressure. The shell is supposed to be initially in equilibrium under the action of an internal pressure and surface tension. The temperatures of the inner and outer shell surfaces are assumed to be fixed at all time. Initially, the

temperature distribution corresponds to steady heat conduction within the shell. The influences of inertia, conductivity, dissipation and surface tension on the shell will be examined by varying *Re*, *Pe*, *Br* and *Ca*, respectively. The accuracy of the numerical implementation is also assessed. In all results reported here, the value of the initial aspect ratio is fixed at $R_r = 1$, which corresponds to a relatively thick shell. The level of pressure is reflected in the value of *Re*. The outer surface is assumed to remain at a colder temperature, $T(S,t) = 1$, while the inner surface at a hotter temperature, $T(R,t) = 2$. This configuration is encountered in typical cavity growth problems, such as during foam molding and extrusion.

3.1. Overall behavior and numerical assessment

Consider the response in thermal and flow behavior for an inflating shell with moderately small inertia ($Re = 10$), and relatively negligible surface tension ($Ca = 10$). In this case, $Br = Pe = 100$. Fig. 1 displays the evolution of the inner and outer radii $R(t)$ and $S(t)$ with time. The response is typically of the exponential type, and therefore emphasis will be on the early transients. The rate of growth is reflected in Fig. 2 through $\dot{R}(t)$ and $\dot{S}(t)$. It is clear, and as expected, that $\dot{R}(t) > \dot{S}(t)$. In general, the inner surface moves 30% faster than the outer surface, leading to the thinning and eventual breakup of the shell. It is interesting to observe that the outer surface tends to accelerate monotonically with time, while the inner surface experiences a relatively strong acceleration initially. The acceleration of the inner surface, however, diminishes with time, reaching a minimum, but picks up again for $t > 1$. In the long term, the two surfaces accelerate at the same rate.

The evolution of the temperature distribution is shown in Fig. 3, where $T(r,t)$ is plotted against r at different time stages. The temperature tends to exhibit a maximum at any time stage. There is a sharp increase near the inner surface, indicating strong dissipation near

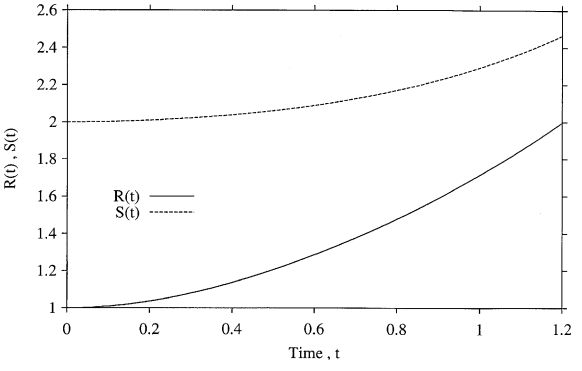

Fig. 1. Evolution of the inner and outer radii, $R(t)$ and $S(t)$ with time for $Br = Pe = 100$, $Ca = Re = 10$ and $R_r = 1$.

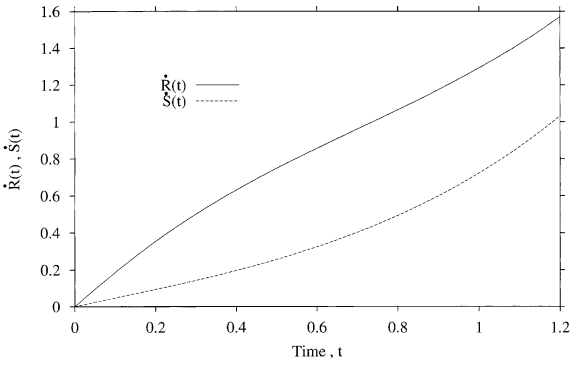

Fig. 2. Evolution of the rate of growth of inner and outer surfaces of the spherical shell, for the same parameter values as in Fig. 1.

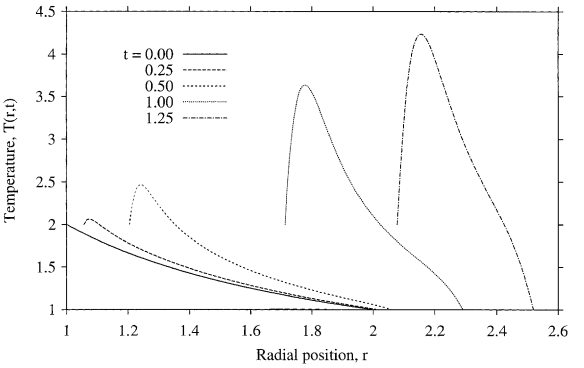

Fig. 3. Temperature distribution across the shell at different time stages, for the same parameter values as in Fig. 1.

$r = R(t)$. The maximum becomes increasingly localized with time because of the thinning of the shell. However, the temperature gradient remains consistently higher near the inner surface. This is resulting from the presence of strong dissipation, which in turn is due to the relative dominance of $\dot{R}(t)$. The evolution of the temperature is further understood from Fig. 4, where $T(x,t)$ is plotted against t at different radial locations between $x = 0$ and $x = 7$ (recall that the interval for x does not change with time). The figure shows that the temperature increases generally with time, except near the inner shell surface, where the temperature reaches a maximum and begin to decrease. The rate of increase is not always monotonic. In particular, the temperature tends to level off near the inner surface, while it tends to grow rapidly elsewhere, except near the outer surface where it remains essentially small. However, the temperature growth rate is uniformly the same upon inception ($t = 0$). The intricate behavior near $r = R(t)$ or $x = 0$ is the result of the interplay among convection, diffusion and dissipation. In order to understand the behavior near the inner surface, first note from Eq. (7) and Fig. 3 the locations

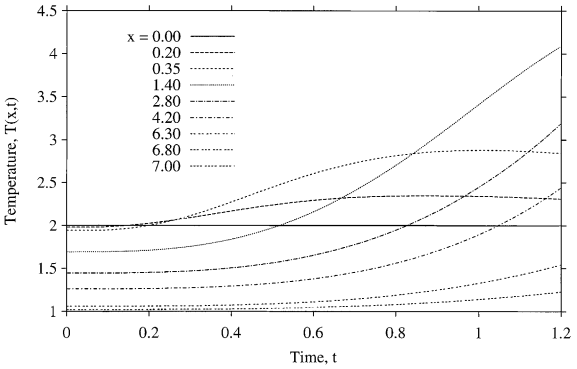

Fig. 4. Evolution of the temperature for different radial locations between $x = 0$ and $x = 7$, for the same parameters as in Fig. 1.

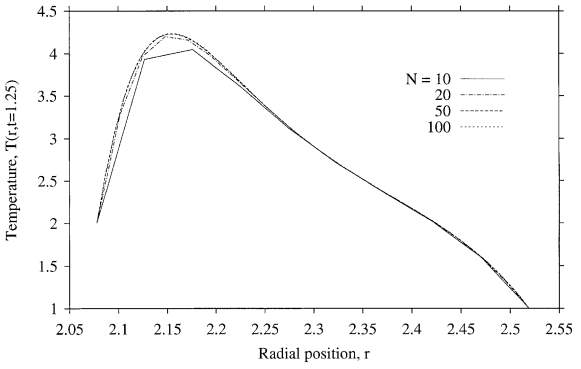

Fig. 5. Influence of number of mesh size on the temperature distribution at $t = 1.25$ for the same parameter values as in Fig. 1.

$x = 0.2$ and 0.35 are essentially upstream of where the maximum in temperature occurs. In this region, the temperature gradient is very steep and positive, thus making the convective effect dominant. Dissipation is also significant since the velocity is large and the radius is relatively small. Thus the convective and dissipative terms in Eq. (7) tend to be in balance with each other, leaving the growth in T essentially proportional to the diffusive term. However, Fig. 3 clearly indicates that the concavity is small near $r = R(t)$ so that the $\partial T/\partial t$ remains eventually constant since it behaves like $T(r = R, t)$. At the location of the maximum in temperature, the rate of growth of T is dictated by the dissipative term, which for the present case ($Pe = Br = 100$) dominates entirely the diffusive term. For a point located further downstream, that is after the maximum in temperature is reached, the convective term becomes increasingly important (as r increases), but this time its effect adds to dissipation, leading to the significant growth rate in T that is depicted in Fig. 4.

The accuracy of the method is mainly influenced by the spatial discretization of the energy equation. The integration with time is handled practically to any desired accuracy. It is generally found that the influence of the mesh size in the radial direction is rather insignificant. Convergence is essentially achieved by using 50 nodes for $x \in [0, 7]$. Fig. 5 shows the influence of N on the temperature distribution at $t = 1.25$ as in Fig. 3. It is observed that even with $N = 10$, the overall temperature distribution is captured except perhaps near the maximum; for $r > 2.15$. For $N = 20$, the temperature estimated at the mesh nodes is fairly accurate; however, more resolution is needed. The distributions based on $N = 50$ and 100 are essentially identical.

3.2. Influence of inertia on heat transfer

In coupled heat and fluid flow, inertia stems from the convective terms in the momentum and energy equations. The two convective effects can be isolated by varying the Reynolds and Peclet numbers separately. First consider the effect of fluid inertia for $Pe = Br = 100$, and $Ca = 10$. The Reynolds number is taken to cover the range $Re \in [10, 40]$. The flow response is typically illustrated in Fig. 6, where the evolution of R and S is displayed for various levels of inertia. Inertia is even more influential on the rate of change of the inner and outer surfaces, as shown in Fig. 7. The overall influence of Re is nonlinear. The inset in the figure clearly shows that the rate of advance increases strongly with Re in the small range of Reynolds number, and reaches a saturation level as Re increases. A similar response is observed regarding flow dissipation. Indeed, the evolution of $T_{\max}(t)$ in Fig. 8 indicates that the increase in $T_{\max}(t)$ is higher as Re increases. There is, however, a saturation that is reached as reflected in the inset of Fig. 8.

The influence of convective effect is illustrated in Fig. 9, where $T_{\max}$ is plotted against t for $Re = Ca = 10$ and $Br = 100$. Here Pe is taken to vary between 100 and 400.

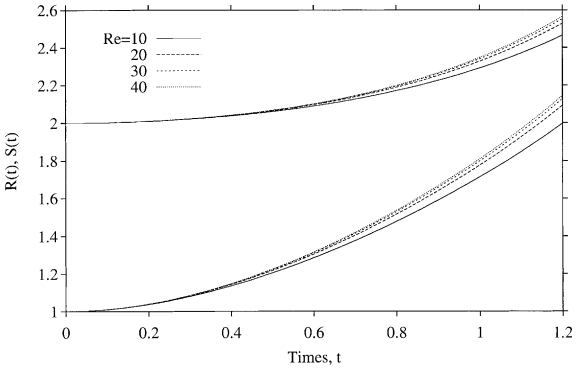

Fig. 6. Influence of fluid inertia on the evolution of the inner and outer radii of the shell for $Pe = Br = 100$, $Ca = 10$, and $Re \in [10, 40]$.

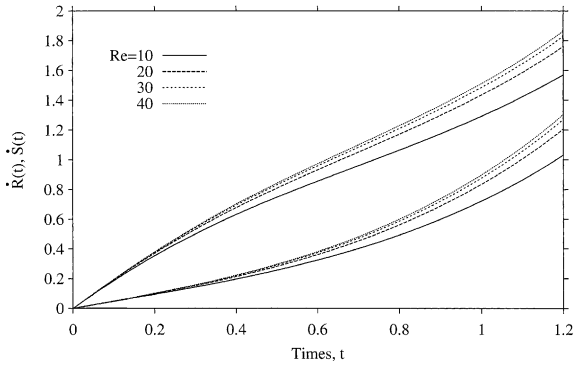

Fig. 7. Influence of fluid inertia on the evolution of the inner and outer surface velocity of the shell for $Pe = Br = 100$, $Ca = 10$, and $Re \in [10, 40]$.

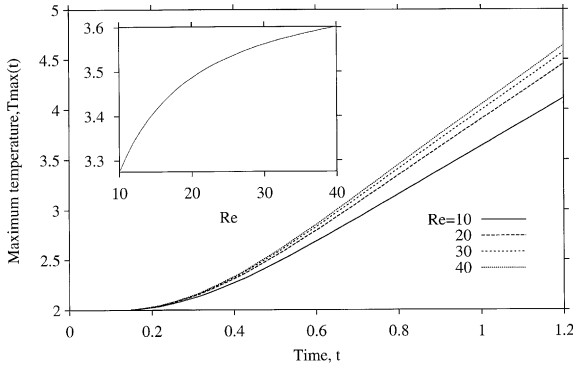

Fig. 8. Influence of fluid inertia on the evolution of the maximum temperature, for $Re \in [10, 40]$, $Br = Pe = 100$, $Ca = 10$ and $R_r = 1$. Inset shows the behavior of $T_{\max}(t = 0.85)$ versus Re.

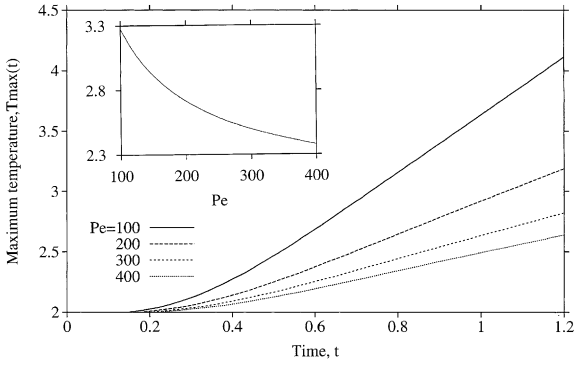

Fig. 9. Influence of the Peclet number on the evolution of the maximum temperature, for $Re = Ca = 10$ and $Br = 100$, while Pe is taken to vary between 100 and 400. The inset $T_{\max}(t = 0.85)$ against Pe.

The figure shows that, unlike inertia, convection tends to lower the temperature buildup. An overall assessment is

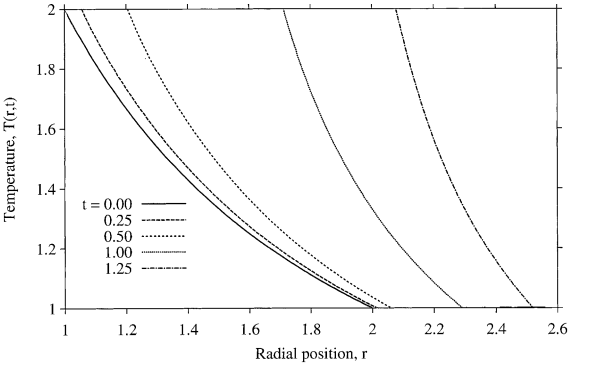

Fig. 10. Temperature distribution across the shell at different time stages, in the absence of energy dissipation, for $Br = 0$, $Pe = 100$, $Ca = Re = 10$ and $R_r = 1$.

inferred from the inset. The temperature drops sharply with Pe in the small range, but eventually reaches a saturated level in the high range.

3.3. Influence of flow dissipation

The influence of flow dissipation is expected to be significant. In fact, in the absence of dissipation, convective effects will simply reflect the heat transport across the shell as if only heat conduction were present. In fact, Fig. 10 displays the temperature distributions at different time stages for $Br = 0$. In this case, the temperature at a point across the shell does not vary with time. The distributions in Fig. 10 correspond to steady heat conduction over the shell thickness as the shell decreases with time. These distributions should be compared with those in Fig. 3 ($Br = 100$).

The influence of dissipation is typically illustrated in Fig. 11, where the evolution in the temperature

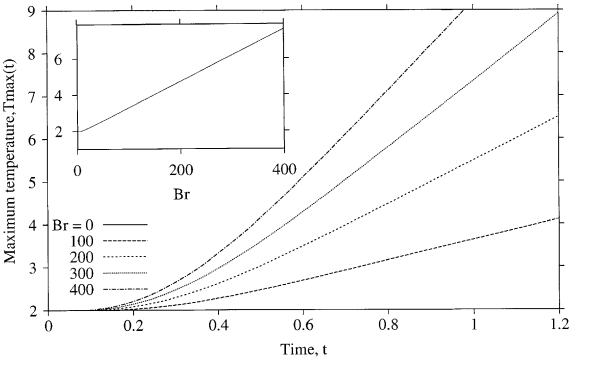

Fig. 11. Influence of energy dissipation on the evolution of the maximum temperature, for $Br \in [0, 400]$, $Pe = 100$, $Ca = Re = 10$ and $R_r = 1$. The inset shows $T_{\max}(t = 0.85)$ versus the Brinkman number.

maximum is shown for $Br \in [0, 400]$. As expected, $T_{max}(t)$ increases with both t and Br. More importantly, the increase in the temperature is linear with dissipation (see inset). This is not surprising since the flow, and therefore the dissipative term in Eq. (7), is decoupled from the temperature. Thus, the dissipative term in the energy equation plays the role of a heat source.

3.4. Influence of surface tension

Similarly to inertia, surface tension is expected to affect significantly the dissipation within the fluid, and therefore the temperature. However, while inertia tends to accelerate the flow, surface tension tends to delay it. The influence of surface tension on the heat transfer depends solely on the square of the radial velocity. Thus the heat transfer for a growing or collapsing shell can be similar if the magnitude of the velocities in the two cases is the same. However, the flow dynamics for a growing shell can be significantly different from that of a collapsing shell. Once a driving pressure is imposed, surface tension becomes the sole parameter that dictates whether a shell will subsequently grow or collapse.

The influence of surface tension on the flow is illustrated in Figs. 12 and 13, where the evolution of the radius and velocity are, respectively, shown for $Re = 10$, $Pe = Br = 100$, and $Ca \in [0.1, 40]$. It is generally clear that, for a given Reynolds number, a critical Ca value exists at which the internal (gas) pressure is permanently balanced by surface tension; in this case, the shell does not move for $Ca = 0.3$ ($Re = 10$). Fig. 12 displays the evolution of R and S for a growing shell ($Ca > 0.3$), and a collapsing shell ($Ca < 0.3$). Surface tension clearly prohibits growth. There is a saturation of the effect of surface tension for $Ca > 10$. The curves corresponding to $Ca = 0.2$ and 0.1 reflect a collapsing shell. In fact, for $Ca = 0.1$, the shell collapses entirely at $t > 0.5$. More importantly, the velocity at which the collapse occurs is significantly large, as shown in Fig. 13. There is a strong acceleration for $t > 0.5$, which is bound to give rise to a strong dissipation in the fluid.

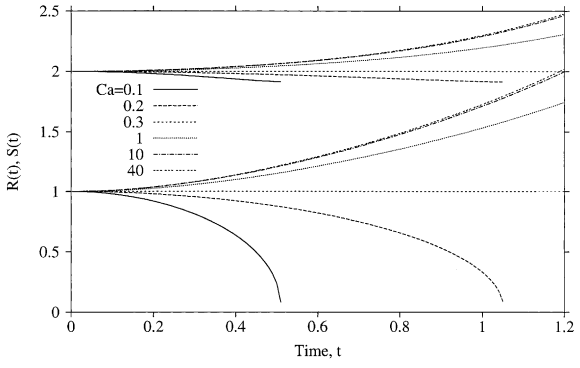

Fig. 12. Influence of surface tension on the evolution of the inner and outer suface radii for $Re = 10$, $Pe = Br = 100$ and $Ca \in [0.1, 40]$. The figure indicates that the shell grows for $Ca > 0.3$, and collapses for $Ca < 0.3$.

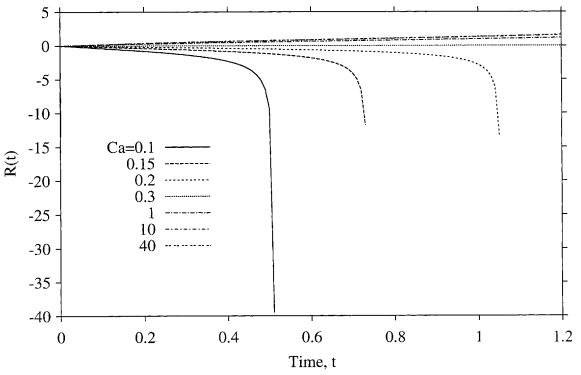

Fig. 13. Influence of surface tension on the rate of growth of the inner surface for $Re = 10$, $Pe = Br = 100$ and $Ca \in [0.1, 40]$.

In general, the critical capillary number, when no growth or collapse occurs, is given from the equilibrium relation that holds initially between inertia (pressure) and surface tension effects. Under equilibrium conditions, Eq. (14) reduces to

$$Re - \frac{2}{Ca}\left[\frac{1}{R(0)} + \frac{1}{S(0)}\right] = 0, \tag{23}$$

where $R(0)$ and $S(0)$ are given from conditions (15) and (19) to give the relation

$$Re = \frac{2}{Ca}\left(\frac{R_r + 2}{R_r + 1}\right). \tag{24}$$

It is clear that when $Re = 10$ and $R_r = 1$, then $Ca = 0.3$ as indicated in Fig. 12.

The influence of Ca on the evolution of the temperature is depicted from Fig. 14. The correlation between the temperature and velocity is clear. The weakest rise in

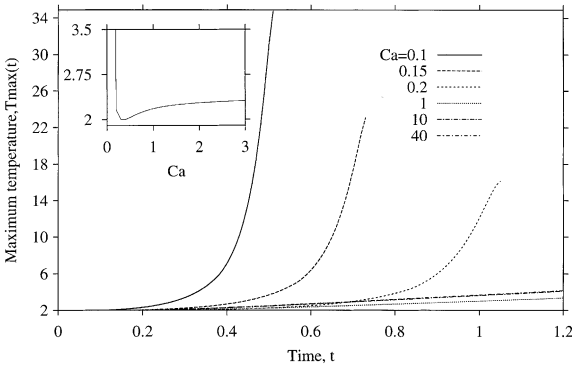

Fig. 14. Influence of surface tension on the evolution of the maximum temperature. Note that no temperature buildup occurs for $Ca = 0.3$. The inset shows $T_{max}(t = 0.45)$ versus Ca.

T occurs for $Ca = 0.2$, which corresponds to the weakest (non-zero) velocity. Note that when $Ca = 0.3$, surface tension balances completely the driving pressure. In this case there is no growth or collapse of the shell, and no temperature buildup. Fig. 14 shows that the temperature decreases slowly with surface tension for a growing shell, reaching a minimum at $Ca = 0.3$. As surface tension becomes more significant, with Ca decreasing further, the shell collapses and the temperature increases sharply as indicated in the figure and the inset. This jump in T is the result of the significant dissipative effects reflected in Fig. 13.

4. Conclusion

The present study focuses on the transient heat transfer during the growth and collapse of spherical shells of a viscous Newtonian fluid, under the action of constant driving pressure. The thermo-mechanical coupling is expected to emerge in processing such as foaming and blow molding. The influence of inertia, viscous dissipation, and surface tension effects is particularly emphasized, with close examination of the temperature buildup during flow. It is found that the maximum temperature distribution exhibits a logarithmic dependence on Reynolds number, a parabolic decay with Peclet number, and a linear growth with Brinkman number shown. Surface tension adds significantly to the buildup of temperature.

Acknowledgements

This work is supported by the Natural Sciences and Engineering Research Council of Canada.

References

[1] A.B. Strong, Plastics: Materials and Processing, second ed., Prentice Hall, Upper Saddle River, NJ, 2000.
[2] M.E. Ryan, A. Dutta, Polym. Eng. Sci. 22 (1983) 569.
[3] S.K. Goel. Ph.D. Thesis, University of Pittsburgh, Pittsburgh, Pennsylvania, 1993.
[4] R.P. Chhabra, Bubble, Drops, and Particles in Non-Newtonian Fluid, CRC Press, Boca Raton, FL, 1993.
[5] H.S. Fogler, J.D. Goddard, Collapse of spherical cavities in viscoelastic fluids, Phys. Fluids 13 (1970) 135.
[6] I. Tanasawa, W.J. Yang, Dynamic behavior of a gas bubble in viscoelsatic liquids, J. App. Phys. 41 (1970) 4526.
[7] R.Y. Ting, Viscoelastic effect of polymers on single bubble dynamics, AIChE J. 21 (1975) 810.
[8] R.B. Bird, R.C. Armstrong, O. Hassager, Dynamics of Polymeric Liquids, vol. 1, second ed., John Wiley and Sons, New York, 1987.
[9] G.H. Pearson, S. Middleman, AIChE J 23 (1977a) 714.
[10] G.H. Pearson, S. Middleman, AIChE J. 23 (1977b) 722.
[11] E.D. Johnson, S. Middleman, Polym. Eng. Sci. 18 (1978) 963.
[12] R.E. Khayat, A. Garcia-Rejon, Uni- and bi-axial unsteady inflation of a viscoelastic material, J. Non-Newtonian Fluid Mech. 43 (1992) 31.
[13] R.E. Khayat, Oscillatory behavior in statically stressed viscoelastic inflation flow, Quart. J. Mech. App. Math. 54 (2001) 599.
[14] A. Shafi, R.W. Flumerfelt, Initial bubble growth in polymer foam process, Chem. Eng. Sci. 52 (1997) 627.
[15] K. Jacobsen, D. Pierick, Microcellular foam molding: advantages and application examples, in: SPE Annual Technical Conference, this volume, 2000.
[16] E.J. Barlow, W.E. Langlois, IBM J. 6 (1962) 329.
[17] J.R. Street, A.L. Fricke, L.P. Reiss, Ind. Eng. Chem. Fund. 10 (1971) 54.
[18] C.D. Han, H.J. Yoo, Polym. Eng. Sci. 21 (1981) 518.
[19] M. Amon, C.D. Denson, Polym. Eng. Sci. 24 (1984) 1026.
[20] M. Amon, C.D. Denson, Polym. Eng. Sci. 26 (1986) 255.
[21] A. Arefmanesh, S.G. Advani, Diffusion-induced growth of a gas bubble in a viscoelastic fluid, Rheol. Acta 30 (1991) 274.
[22] A. Arefmanesh, S.G. Advani, Nonisothermal bubble growth in polymeric foams, Polym. Eng. Sci. 35 (1995) 252.
[23] G.K. Batchelor, Introduction to Fluid Dynamics, Cambridge University Press, Cambridge, 1961.
[24] W.C. Park, G. Homsy, Two-phase displacement in Hele-Shaw cells; theory, J. Fluid Mech. 139 (1984) 291.
[25] P.S. Epstein, M.S. Plesset, On the stability of gas bubbles in liquid–gas solutions, J. Chem. Phys. 18 (1950) 1505.